Perpendicular Grating Coupler Based on a Blazed Antiback-Reflection Structure

Tatsuhiko Watanabe, *Member, IEEE*, Masafumi Ayata, Ueli Koch, Yuriy Fedoryshyn, and Juerg Leuthold, *Fellow, IEEE*

***Abstract*—Silicon photonic grating couplers are demonstrated featuring a perfect vertical coupling and predicted coupling efficiencies of 87% and 78% with an apodized and a standard periodic structure, respectively. Vertical coupling is usually difficult to be achieved with standard diffraction gratings, since both the forward and backward scattered light meet the Bragg condition alike. In this work a vertical grating coupler which satisfies both high directionality ($> 97\%$) and low back-reflection ($< 1\%$) simultaneously is realized using a blazed sub-wavelength structure. The measured maximum coupling efficiencies with a standard single-mfiber are -1.5 dB and -2.2 dB for apodized and periodic structures, respectively. The suggested structure offers an ultimate solution for compact coupling schemes in Si photonics, since it meets the most important needs of grating couplers, which are directionality, ease of fabrication, and a possibility to vertically couple. The vertical grating coupler are fabricated on a silicon-on-insulator wafer with a 220 nm-thick silicon layer, relying only on a 2-step etching technology.**

***Index Terms*—Grating coupler, high directionality, integrated photonics, Si photonics, vertical coupler.**

I. Introduction

PERFECT vertical grating couplers are of high interest since they allow for an easy alignment of vertically aligned fibers and fiber arrays to couple light to horizontal waveguides on a chip. A prominent example are emerging space division multiplexing (SDM) schemes. SDMs [1], [2] promise a dramatic increase of the transmission capacity in long-haul optical fiber communications because they can guide multiple independent signals. However, to make SDM transmission systems practical, multi-core fibers (MCFs) in which multiple cores are densely packed have been proposed [3]–[6]. And indeed, SDM technology is expected to be a solution to increase the degree of integration and parallelism in optical interconnects [7], [8].

To achieve a dense coupling density fan-in/fan-out (FI/FO) devices for multi-core fibers (MCFs) have recently been demonstrated with a two-dimensional array of silicon grating couplers [9]–[11]. Similarly, polarization splitters [12] and mode multiplexers for few-mode fibers (FMFs) [13], [14] have also been realized using a grating coupler array. These device concepts could be more promising than other multiplexing devices such as a photonic lantern [15], provided that efficient perfect vertical grating couplers were utilized. However, with a standard grating coupler the fiber has to be aligned at a particular coupling angle with respect to the surface of the chip in order to suppress back-reflections. Therefore each grating coupler in these array devices was forced to be arranged facing an identical direction to maintain the coupling angles, resulting in a restriction of the channel density. For instance, to couple a 37-core fiber with the array devices, bus-waveguides of grating couplers have been obliged to taper down within a length of the core pitches of the MCF (i.e., 40 μm) in Ref. [10]. To arrange seven grating couplers, a 45deg.-slants waveguide which enables routing 13μm-width bus-waveguides has been adopted to arrange seven grating couplers [11]. On the other hand, a tilt-free grating coupler could provide freely arranged routing bus-waveguides as envisioned in Fig. 1. If such a scheme with efficient vertical grating coupler were available it likely would become a key component that could significantly enhance the integration density in silicon photonics.

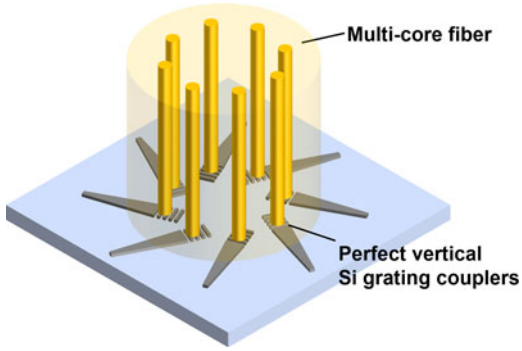

Fig. 1. Schematic view of a fan-in/fan-out device for multicore fibers using a grating coupler array with freely routing bus-waveguides.

So far, several efficient fiber-to-chip couplers with perfect vertical coupling have been demonstrated, including 45-degree mirror waveguides based on silica [16] and InP [17] platforms, a bent waveguide technology [18] or vertical grating couplers. There is a rich literature about vertical grating couplers. So for instance, they have been realized by means of an overlay

Manuscript received April 18, 2017; revised June 30, 2017 and August 14, 2017; accepted August 31, 2017. Date of publication September 21, 2017; date of current version October 12, 2017. This work was supported in part by the ERC PLASILOR under Grant 67048, in part by Grant-in-Aid for JSPS Research Fellow 26-198, and in part by Japanese-Swiss Science and Technology Programme. *(Corresponding author: Tatsuhiko Watanabe.)*

The authors are with the Institute of Electromagnetic Fields, ETH Zurich, Zurich 8092, Switzerland (e-mail: watanabt@ethz.ch; masafumi.ayata@ief.ee.ethz.ch; ueli.koch@ief.ee.ethz.ch; yuriy.fedoryshyn@ief.ee.ethz.ch; juerg.leuthold@ief.ee.ethz.ch).

Color versions of one or more of the figures in this paper are available online at http://ieeexplore.ieee.org.

Digital Object Identifier 10.1109/JLT.2017.2755673

TABLE I
FIGURES OF MERIT OF VERTICAL GRATING COUPLERS

Year	Coupling efficiency [%]		Grating Height [nm]	Apd.	Pol.	Fabrication steps		Ref.
	Sim.	Exp.				Etch.	Dep.	
2005	76	-	240	-	TE	1*	-	[21]
2007	50	-	370	-	TE	1	1	[19]
2008	42	34	220	✓	TE	1	-	[22]
2013	68	60	343	✓	TE	1	4	[23]
2015	70	-	300	-	TE	2	2	[20]
2015	24	22	340	✓	TM	1	-	[24]
2017	78	60	220	-	TE	2	-	This work
	87	71		✓				

Sim.: Simulated, Exp. : Experimental, Apd. ; Apodized (incl. Chirped), Pol. : Polarization, Etch. : Etching, Dep. : Deposition.
*Side walls of etching must be slanted.

technology [19], a dual layer waveguide scheme [20] or a slanted tilted waveguide [21]. While simulations predict coupling efficiencies up to 76% practical realizations have shown coupling efficiencies up to 60% [21]–[24]. A while these are already good results so far most published vertical coupling schemes require intricate fabrication steps and often require additional fabrication steps that are not compatible with the conventional CMOS platform. Table I summarizes figures of merit of reported vertical grating couplers. In Table I, the term "Coupling efficiency" relates to a coupling efficiency with standard single-mode fibers (SMF) and a mode field diameter of around 10 μm. "Fabrication steps" represents the number of fabrication steps to form the grating structure on a SOI wafer with the core layer and the buried oxide (BOX) layer already deposited. Here, the number of deposition steps (Dep.) excludes top-cladding layer deposition.

On the other hand, highly efficient grating couplers have been demonstrated with blazed and sub-wavelength structures, even though they need particular tilt angles of the fiber for coupling. In Ref. [25], a sub-wavelength structure has been adopted to suppress the back-reflection. Then, very recently, a grating coupler with a coupling efficiency of 78% and a directionality higher than 95% was predicted utilizing the blazing effect with conventional simple fabrication methods [26].

In this paper, we demonstrate a grating coupler providing both a high directionality and perfect vertical coupling from a single-mode fiber (SMF) to a silicon-on-insulator (SOI) waveguide, by adopting both blazed and anti-back-reflection structures in the same grating. While simulations predict coupling efficiencies of 87% in an ideal structure we experimentally show coupling losses of the grating coupler with a SMF of 1.5 dB at the peak wavelength. The coupling technique relies only on a simple double etching process and is compatible with a standard SOI technology.

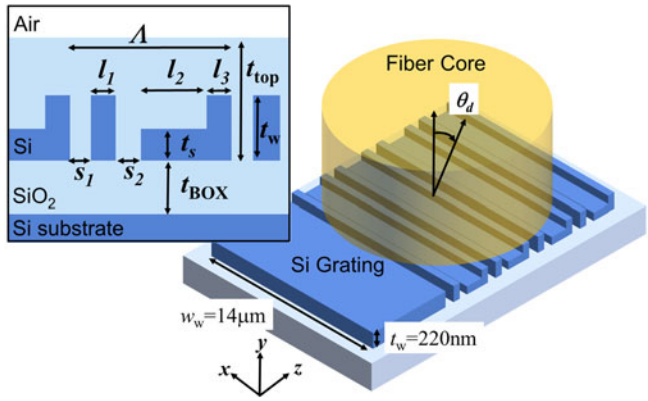

Fig. 2. Schematic view and structural parameters of proposed grating coupler.

II. DESIGN AND CONCEPT OF THE BLAZED GRATING WITH ANTIBACK-REFLECTION STRUCTURES

To achieve a high coupling efficiency several design requirements have been combined into the grating coupler. Vertical coupling is normally difficult to be achieved with a standard diffraction grating, since the forward and backward scattered light undergo the same Bragg condition. Therefore, we integrated a two etch-step blazed and subwavelength grating structure to obtain a low back-reflection and a high directionality. Fig. 2 shows a schematic representation of the proposed grating coupler. Each grating period consists of a single pillar and an L-shaped structure. To enhance the blazing effect the optical path length difference within the L-shaped structure has been optimized for maximum directionality. Furthermore, the subwavelength pillars provide an anti-reflection effect and the back-reflection is suppressed by destructive interference of the reflected light. As a result, our grating coupler achieves both a high directionality and a perfect vertical coupling.

First, the grating coupler was optimized using a commercial FDTD solver (by Lumerical). In the simulation, a waveguide mode with transverse electric (TE) polarization was launched into the grating coupler. The radiated field from the grating coupler was collected with a standard SMF (core diameter: 9.0 μm, index contrast: 0.36%) at an angle of 0 degrees with respect to y-axis (i.e., $\theta_{\mathrm{d}} = 0$). Then, the structural parameters l_1, l_2, l_3, s_1, and s_2 were optimized using the particle swarm algorithm for achieving the maximum optical power coupling into the fiber at the wavelength of 1550 nm. We assumed that the grating coupler is covered by SiO_2 as a top-cladding layer and the refractive indices of Si and SiO_2 were 3.45 and 1.45, respectively. The waveguide width w_{w} and thickness t_{w} were set to 14 μm and 220 nm, respectively. The thickness of shallow etched areas of L-shaped structures, t_{s}, was set to 110 nm. Here, we also simulated and optimized the grating coupler with a shallow etching depth of 70 nm ($t_{\mathrm{s}} = 150\,\mathrm{nm}$) which Si photonics foundries have adopted commonly. The obtained optimal structural parameters are summarized in Table II, where grating periods are defined as Λ. Fig. 3 shows an electromagnetic field profile radiated by the grating coupler with optimum structural parameters summarized

TABLE II
OPTIMUM STRUCTURAL PARAMETERS OF THE GRATING

	l_1	l_2	l_3	s_1	s_2	Λ
t_s=110nm	83nm	314nm	109nm	95nm	112nm	713nm
t_s=150nm	87nm	240nm	154nm	81nm	101nm	663nm

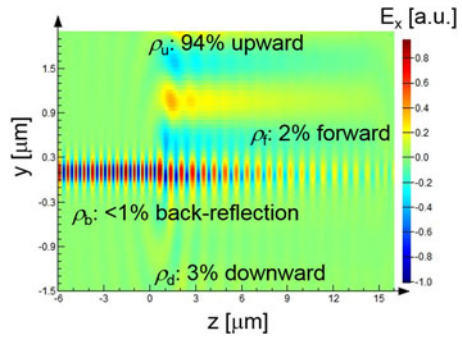

Fig. 3. Simulated electromagnetic field profile radiated by optimized grating coupler.

in table II. In Fig. 3, ρ_{u}, ρ_{f}, ρ_{b}, and ρ_{d} are optical power ratios of lights propagated upward, forward, downward, and backward to the input optical power, respectively. It can be seen from Fig. 3 that the most of the optical power is radiated upward for the grating coupler with the diffraction angle of 0 degrees at the wavelength of 1550 nm. Here, the directionality η_{D} is defined as

$$\eta_{\mathrm{D}} = \rho_u/(\rho_u + \rho_d). \tag{1}$$

Thus, the directionality of the optimized grating coupler is 97%. The back-reflection was sufficiently suppressed to less than 1%.

Furthermore, to investigate dependences of the directionality and the back-reflection on the grating structure, the grating was simulated with varying parameters of the pillar and L-shaped structures. First, the calculations were performed for variations of the width of the shallow etched areas l_2 in the L-shaped structure. Here, a deviation of the width l_2 was defined as dl_2 so that,

$$l_2 = l_{2,0} + dl_2, \tag{2}$$

$$l_3 = l_{3,0} - dl_2, \tag{3}$$

where parameters with subscript "0" such as $l_{2,0}$ represent the ideal value summarized in Table II. Here, parameters other than l_2 and l_3 were maintained at optimum values. It can be seen from Fig. 4(a) that the directionality is strongly affected by the width of the shallow etched area of the L-shaped structures. In contrast fluctuations of back-reflections are below 8%. Second, the calculations were performed for various pillar structure parameters with deviations of dl_1 in the following equations,

$$l_1 = l_{1,0} + dl_1, \tag{4}$$

$$s_1 = s_{1,0} - dl_1. \tag{5}$$

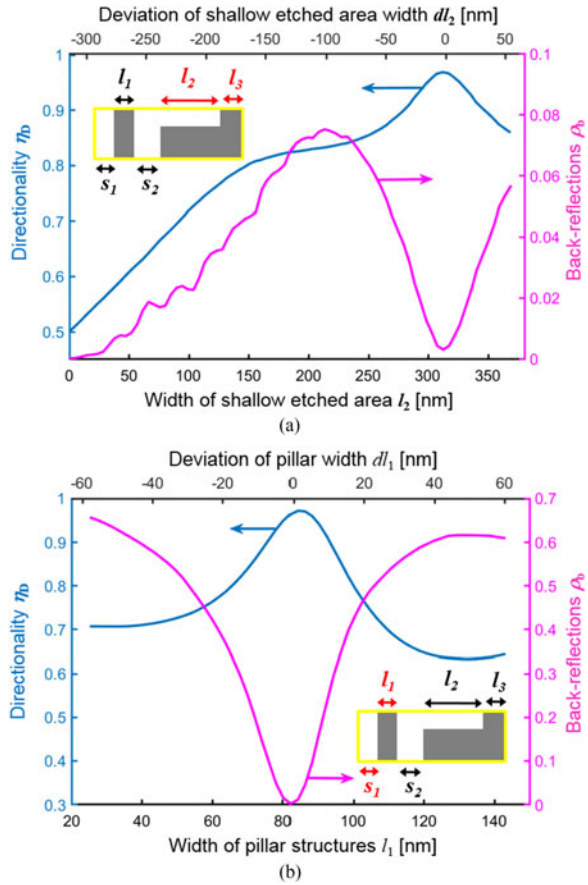

Fig. 4. Dependences of the directionality and the back-reflection on structural parameters of gratings. (a): L-shaped structures, (b): pillar structures.

As shown in Fig. 4(b), the back-reflection is highly dependent upon the pillar width. The backward reflected light increases if the pillar width is not properly chosen and is diffracted downward by means of the blazing effect of L-shaped structures. As a result, the directionality is deteriorated even though the L-shaped structures are maintained at an ideal geometry. Therefore one can infer that the directionality is determined by the L-shaped structure that is responsible for the blazing effect and the pillar structures play an important role for suppressing back-reflections.

Next, we investigated dependences of the directionality and the back-reflection on the BOX layer thickness. Since downward diffracted light is reflected at the Si substrate surface one might expect that the power of the upward light fluctuates due to interference of with downward back-reflected light when varying the thickness of the BOX layer. However, our grating coupler has a sufficiently high directionality so that one only finds a very small dependence on the BOX layer thickness. As shown in Fig. 5, directionality fluctuations were below 1% and back-reflection was hardly influenced by the BOX thickness.

Subsequently, fabrication tolerances of the coupling efficiency η_{CE} were studied. The coupling efficiency of a grating coupler is defined as the ratio of the optical power coupled into an SMF P_{SMF} to the power of TE polarized fundamental mode

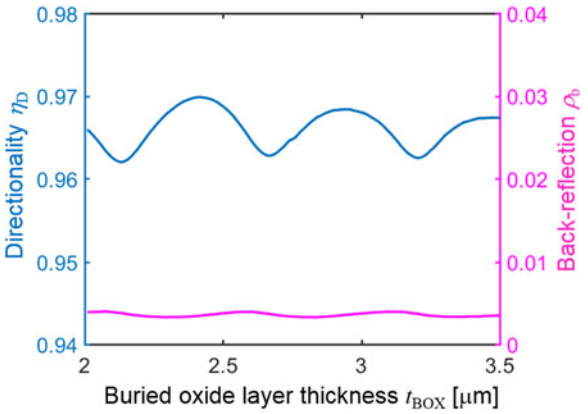

Fig. 5. Dependences of the directionality and the back-reflection as a function of the thickness of buried oxide layer.

in the waveguide P_{W}. This way the coupling efficiency can be expressed as,

$$\eta_{CE} = \frac{P_{\mathrm{SMF}}}{P_{\mathrm{W}}} = \phi_{\mathrm{FO}} \cdot \rho_u \cong \phi_{\mathrm{FO}} \cdot \eta_{\mathrm{D}} \cdot (1 - \rho_{\mathrm{b}} - \rho_{\mathrm{f}}), \quad (6)$$

where, ϕ_{FO} is an overlap coefficient between a mode field profile of the SMF and that radiated by the grating coupler, ρ_{b} and ρ_{f} are the ratio of optical power back-reflected by gratings and passing through gratings, respectively. Both ρ_{b} and ρ_{f} can assumed to be small numbers.

Since fabrication errors of the grating width and the thickness of the shallow etched area are expected in fabrication, the coupling efficiency was calculated for the case where they would deviate from the ideal value as a function of wavelength. Here, width errors of gratings that might be caused by full and shallow etchings were assumed to be dl_{F} and dl_{S}, respectively. An error of etching depth of the shallow etched area was defined as dt_{S}. Then, each deviation from the ideal grating can be expressed as,

$$s_1 = s_{1,0} - dl_{\mathrm{F}}, \quad (7)$$

$$s_2 = s_{2,0} - dl_{\mathrm{F}}, \quad (8)$$

$$l_1 = l_{1,0} + dl_{\mathrm{F}}, \quad (9)$$

$$l_2 = l_{2,0} + dl_{\mathrm{F}}/2 - dl_{\mathrm{S}}/2, \quad (10)$$

$$l_3 = l_{3,0} + dl_{\mathrm{F}}/2 + dl_{\mathrm{S}}/2, \quad (11)$$

$$t_s = t_{\mathrm{s},0} + dt_{\mathrm{S}}. \quad (12)$$

As shown in Fig. 6(a), the peak wavelengths of the coupling efficiency is shifting with the width variation. This can be understood as follows. From the diffraction principle it is clear that an increase of the grating width results in an increase of the effective refractive index of the grating area which corresponds to a red-shifting of the peak wavelength. Also, it can be seen from Fig. 6 that the fabrication tolerance of the shallow etched area, Fig. 6(b), is higher than that of the full etched area, Fig. 6(a). Fig. 7 shows the calculated results of the coupling efficiency against changes of the shallow etched area thickness. A

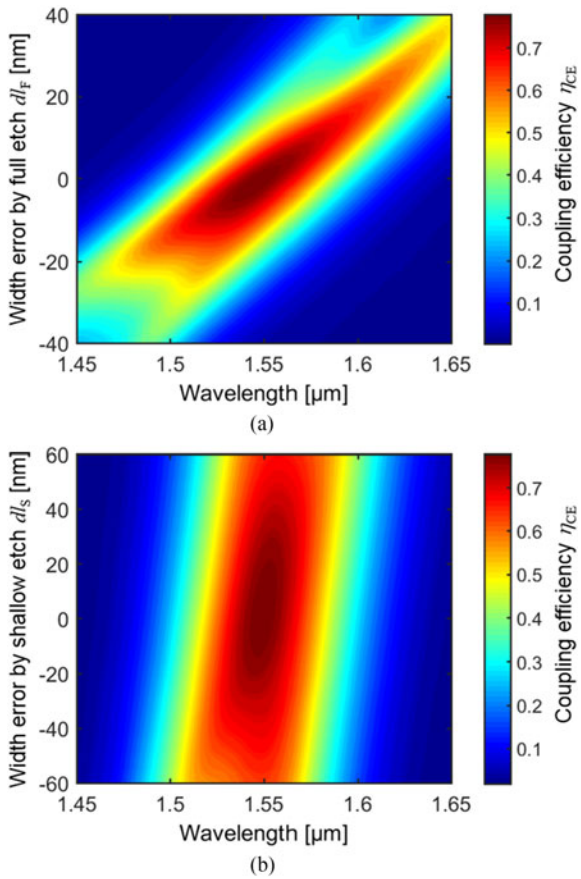

Fig. 6. Fabrication tolerances of the coupling efficiency. (a)Width error caused by full-depth etching process. (b)Width error caused by shallow-depth etching process.

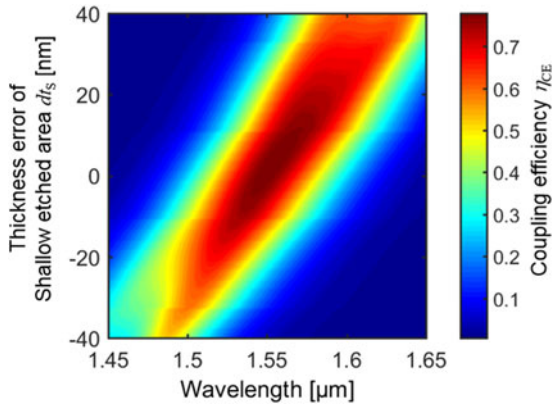

Fig. 7. Dependence of coupling efficiency on thickness errors of the shallow etched area.

coupling efficiency of $> 60\%$ can be maintained for deviations of $< \pm 10$ nm at the wavelength of 1550 nm.

Finally, we simulated top-cladding thickness dependence of the coupling efficiency as shown in Fig. 8. Here, the refractive index of the background area of the simulation was set to 1.0 as the one of the air. The grating was covered by silica cladding with a thickness of t_{top}. Fluctuations of the coupling efficiency due to interferences of light reflected at the cladding surface

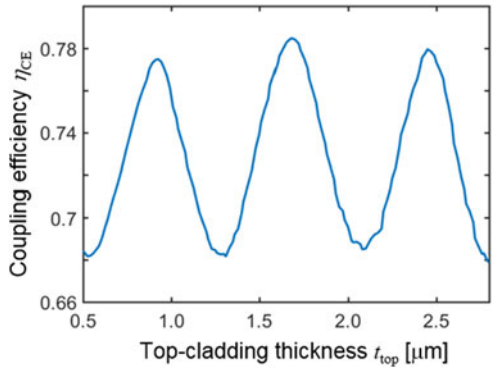

Fig. 8. Coupling efficiency dependence on top-cladding thickness.

can be observed in Fig. 8. Fluctuations are in a range of about 10%. Under consideration of the results from Fig. 8 we fixed the top-cladding thickness t_{top} to 1.7 μm.

III. Apodization

It is shown in Eq. (6) that the coupling efficiency of grating couplers with a standard SMF can be considered as a product between the overlap coefficient ϕ_{FO} and the directionality η_{D}, assuming ρ_{b} and ρ_{t} are negligible. Above we have optimized η_{D} but there is room in improving the overlap coefficient ϕ_{FO}. ϕ_{FO} is the result of the overlap between mode profile emitted by the grating and the mode profile in the single mode fiber. The periodic grating coupler produces an exponentially decaying intensity profile along the propagation direction (z direction in Fig. 2) [27]. In contrast, the profile of a fundamental mode of an SMF has approximately a Gaussian shape. In order to further enhance the coupling efficiency, we have engineered the field distribution using apodization [27], [28].

Our grating coupler has 20 periods of gratings and each grating has 5 structural parameters (i.e., 100 variables in total). To solve such an optimization problem with many variables, we have adopted the evolutional strategy [29]. First, the variables were thinned out, so that each grating parameter can be defined by a spline function with 6 sampling points [30], plotted with rhombus shaped dots in Fig. 9. Then, we only optimized these sampling points using an evolution strategy. The optimized parameters of the apodized grating coupler are shown in Fig. 9, where the parameters of grating coupler with 70 nm-depth shallow etching was apodized. It is noted that this sampling method could be very useful for apodizing a grating coupler with even more parameters.

IV. Fabrication and Characterization

The grating couplers were fabricated on a commercially available SOI wafer with a 220 nm-thick Si and 3.0 μm-thick BOX layer. First the shallow etched areas of the grating coupler were defined by electron-beam (EB) lithography (Vistec EBPG5200) using a positive-tone resist, followed by dry-etching with HBr-ions (Oxford Plasmofab System 100). Next, the waveguides and full-etched regions of the device were processed with negative-tone resist and dry-etching with HBr-ions. Judging from a

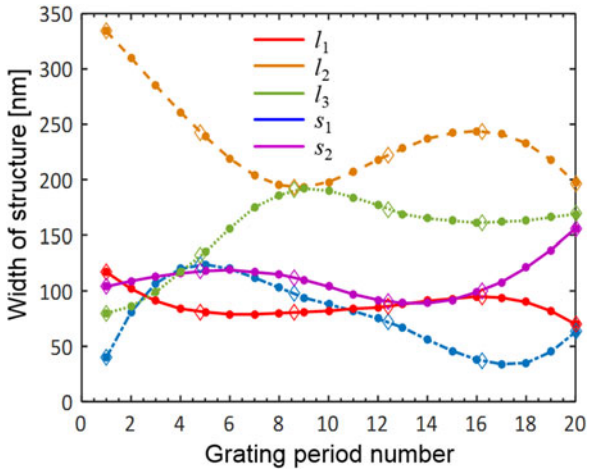

Fig. 9. Optimized parameters of the apodized grating coupler. The dimensions of search space can be reduced from 100 to 30 by optimizing only the sampling points plotted with rhombus dots.

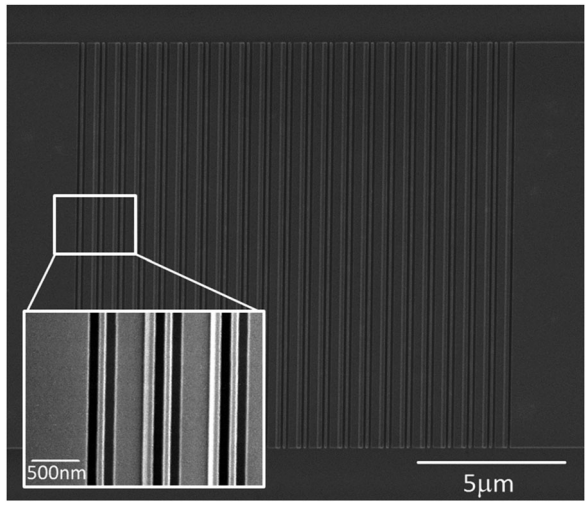

Fig. 10. Scanning microscopy image of the fabricated periodic grating coupler with 110 nm-depth shallow etching. The white window represents magnified gratings.

scanning electron microscopy (SEM) image of the fabricated grating coupler the pillars and L-shaped structures have been well formed as shown in Fig. 10. Then, a top-cladding layer of silica was deposited using PECVD (Oxford Plasmalab System 100). We fabricated two chips. One was with 110 nm-depth shallow etching and the other was with 70 nm-depth shallow etching. The apodized grating was fabricated with a 70 nm-depth shallow etching.

The fabricated devices have been characterized with vertically aligned two single mode fibers. The device consist of input and output grating couplers with a 200 μm long tapering waveguide. These two grating couplers were connected via a 500 nm wide waveguide with a length of several millimeters (3.6 mm for one with 110 nm-depth shallow etching and 4.8 mm for ones with 70 nm-depth shallow etching). The insertion loss (fiber-to-device-to-fiber) were measured using a tunable laser source and a power meter. The polarization of the incident light was

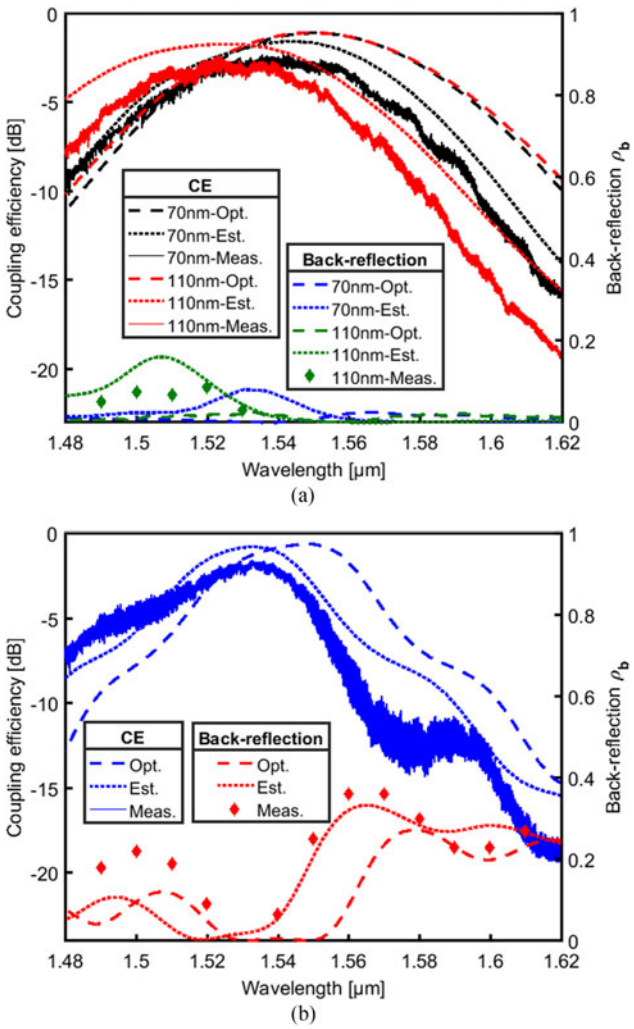

Fig. 11. Measured and simulated coupling efficiencies and back-reflections of periodic (a) and apodized (b) grating couplers as a function of wavelength. Solid lines represent measured (Meas.) values. Dashed lines represent theoretical values with optimum structures (Opt.). Dotted lines represent theoretical values estimated using fabricated structures (Est.). Diamond shaped dots represent experimental back- reflections evaluated by Fabry-Perot ripples of measured spectrums.

adjusted to the TE mode using a polarization controller. The coupling losses of the fabricated grating coupler were evaluated by subtracting the propagation and back-to-back losses from the measured insertion losses.

Fig. 11 summarizes simulated and measured coupling efficiencies of three types of grating couplers (i.e., two periodic grating couplers with 70 nm- and 110 nm-depth shallow etching, and an apodized grating). The simulated coupling efficiencies were –1.1 dB (78%) and –0.6 dB (87%) at 1550 nm wavelength for periodic and apodized gratings, respectively. It can be observed in Fig. 11 that the bandwidth of the apodized grating is narrowed even though the coupling efficiency improved by 9%, compared with the periodic gratings. In this work, the apodization has been optimized for a wavelength around 1550 nm so that the peak coupling efficiency is maximized. Yet, the apodized grating has not been optimized for a broad spectral coupling range. The measured coupling efficiency of the periodic grating couplers with 110 nm-depth shallow etching was –2.4 dB at the peak wavelength of 1522 nm with a 3 dB bandwidth of 66 nm. The one with the 70 nm-depth showed a –2.2 dB coupling loss around 1541 nm wavelength with a 3 dB bandwidth of 69 nm. Finally, the experimental coupling efficiency of the apodized grating coupler was –1.5 dB at a 1533 nm wavelength with a 3 dB bandwidth of 49 nm. The discrepancies of coupling efficiency spectrums between the simulation and the experimental results were expected to be mostly attributed to a narrowing of grating structures during the etching process and thickness errors of the shallow etched areas, resulting in a change of the effective refractive index of the grating area. To confirm this, we simulated coupling efficiencies using structural parameters of the fabricated devices which were observed by SEM images and atomic force microscope, as plotted with dashed lines in Fig. 11. The shifts of peak wavelength can be explained by the structural errors. The discrepancies of the peak coupling efficiency between experiment and estimation were about 0.7 dB for both periodic gratings and the apodized grating.

Furthermore, we also simulated and measured back-reflections as shown in Fig. 11. For periodic grating couplers, the back-reflection can theoretically be suppressed over a wide wavelength range. We evaluated the back-reflection of fabricated grating couplers from Fabry-Perot ripples of the measured coupling efficiency spectrum. For the periodic grating coupler with 110 nm-depth shallow etching, we could calculate back-reflections only at certain wavelengths where the back-reflection is relatively larger ($> \sim 3\%$). The Fabry-Perot ripples caused by the back-reflection were not evident in the spectrum of one with 70 nm-depth shallow etching. As shown in Fig. 11(b), the experimental back-reflections of the apodized grating coupler are fairly-well matched with the estimated values. Since the apodized grating coupler was optimized at the peak-wavelength, the back-reflections are large other than at the peak-wavelength.

V. Conclusion

Highly efficient grating couplers with perfect vertical coupling are successfully demonstrated on a standard SOI wafer with 220 nm-thick silicon layer, relying on a 2-step etching technology. A coupling efficiency of –1.5 dB has been experimentally measured at a wavelength of 1533 nm with a 3 dB bandwidth of 49 nm with an apodized grating coupler structure. We have also shown that our structure effectively suppresses the back-reflection in terms of both simulation and experiment. To the best of our knowledge, this is the highest coupling efficiency experimentally demonstrated with perfectly vertical coupling hitherto without complicated additional fabrication processes. In addition, our grating coupler is compatible with the standard Si photonics technology and is easy to fabricate. Our grating coupler can be a key components that could significantly enhance the integration density in silicon photonics, providing input/output devices of SDM. As an alternative application, our grating coupler can simplify the aligning a chip with an optical-circuit-board (OCB) [31], since the in-plane relative position which minimizes the insertion loss does no more depend on the relative distance between chip and OCB owing to the verticality.

V. Acknowledgment

This work was partially carried out at the Binnig and Rohrer Nanotechnology Center, a joined cleanroom facility of IBM Zurich and ETH Zurich.

References

[1] T. Morioka, "New generation optical infrastructure technologies: 'EXAT initiative' towards 2020 and beyond," in *Proc. Optoelectron. Commun. Conf.*, Hong Kong, 2009, pp. 1–2.

[2] D. J. Richardson, J. M. Fini, and L. E. Nelson, "Space-division multiplexing in optical fibres," *Nat. Photon.*, vol. 7, pp. 354–362, 2013.

[3] H. Takara *et al.*, "1.01-Pb/s (12 SDM/222 WDM/456 Gb/s) crosstalk-managed transmission with 91.4-b/s/Hz aggregate spectral efficiency," in *Proc. Eur. Conf. Exhib. Opt. Commun.*, Amsterdam, The Netherlands, 2012, Paper Th.3.C.1.

[4] J. Sakaguchi *et al.*, "19-core fiber transmission of 19 × 100 × 172-Gb/s SDM-WDM-PDM-QPSK signals at 305 Tb/s," in *Proc. Opt. Fiber Commun.*, Los Angeles, CA, USA, 2012, Paper PDP5C.1.

[5] Y. Amma *et al.*, "High-density multicore fiber with heterogeneous core arrangement," in *Proc. Opt. Fiber Commun. Conf. Exhib.*, Los Angeles, CA, USA, 2015, pp. 1–3.

[6] B. J. Puttnam *et al.*, "2.15 Pb/s transmission using a 22 core homogeneous single-mode multi-core fiber and wideband optical comb," in *Proc. Eur. Conf. Opt. Commun.* Valencia, Spain, 2015, pp. 1–2.

[7] T. Hayashi *et al.*, "125-μm-cladding 8-core multi-core fiber realizing ultra-high-density cable suitable for O-Band short-reach optical interconnects," in *Proc. Opt. Fiber Commun. Conf. Exhib.*, Los Angeles, CA, USA, 2015, Paper Th5C.6.

[8] W. Heni *et al.*, "High speed plasmonic modulator array enabling dense optical interconnect solutions," *Opt. Express*, vol. 23, pp. 29746–29757, 2015.

[9] C. R. Doerr and T. F. Taunay, "Silicon photonics core-, wavelength-, and polarization-diversity receiver," *IEEE Photon. Technol. Lett.*, vol. 23, no. 9, pp. 597–599, May 2011.

[10] V. I. Kopp *et al.*, "Two-dimensional, 37-channel, High-bandwidth ultra-dense silicon photonics optical interface," in *Proc. Opt. Fiber Commun. Conf. Exhib.*, San Francisco, CA, USA, 2014, Paper Th5C.4.

[11] Y. Ding, F. Ye, C. Peucheret, H. Ou, Y. Miyamoto, and T. Morioka, "On-chip grating coupler array on the SOI platform for fan-in/fan-out of MCFs with low insertion loss and crosstalk," *Opt. Express*, vol. 23, pp. 3292–3298, 2015.

[12] X. Chen, C. Li, and H. K. Tsang, "Two dimensional silicon waveguide chirped grating couplers for vertical optical fibers," *Opt. Commun.*, vol. 283, pp. 2146–2149, 2010.

[13] A. M. J. Koonen, H. Chen, H. P. A. v. d. Boom, and O. Raz, "Silicon photonic integrated mode multiplexer and demultiplexer," *IEEE Photon. Technol. Lett.*, vol. 24, no. 21, pp. 1961–1964, Nov. 2012.

[14] B. Wohlfeil, C. Stamatiadis, M. Jager, L. Zimmermann, S. Burger, and K. Petermann, "Integrated optical fiber grating coupler on SOI for the excitation of several higher order fiber modes," in *Proc. Eur. Conf. Opt. Commun.*, Cannes, France, 2014, paper We.1.1.2.

[15] S. G. Leon-Saval, N. K. Fontaine, J. R. Salazar-Gil, B. Ercan, R. Ryf, and J. Bland-Hawthorn, "Mode-selective photonic lanterns for space-division multiplexing," *Opt. Express*, vol. 22, pp. 1036–1044, 2014.

[16] J. Inoue, T. Ogura, K. Kintaka, K. Nishio, Y. Awatsuji, and S. Ura, "Fabrication of embedded 45-Degree micromirror using liquid-immersion exposure for single-mode optical waveguides," *J. Lightw. Technol.*, vol. 30, no. 1, pp. 1563–1568, Jun. 2012.

[17] H. Chen, R. van Uden, C. Okonkwo, and T. Koonen, "Compact spatial multiplexers for mode division multiplexing," *Opt. Express*, vol. 22, pp. 31582–31594, 2014.

[18] T. Yoshida, S. Tajima, R. Takei, M. Mori, N. Miura, and Y. Sakakibara, "Vertical silicon waveguide coupler bent by ion implantation," *Opt. Express*, vol. 23, pp. 29449–29456, 2015.

[19] G. Roelkens, D. V. Thourhout, and R. Baets, "High efficiency grating coupler between silicon-on-insulator waveguides and perfectly vertical optical fibers," *Opt. Lett.*, vol. 32, pp. 1495–1497, 2007.

[20] M. Dai, L. Ma, Y. Xu, M. Lu, X. Liu, and Y. Chen, "Highly efficient and perfectly vertical chip-to-fiber dual-layer grating coupler," *Opt. Express*, vol. 23, pp. 1691–1698, 2015.

[21] W. Bin, J. Jianhua, and G. P. Nordin, "Embedded slanted grating for vertical coupling between fibers and silicon-on-insulator planar waveguides," *IEEE Photon. Technol. Lett.*, vol. 17, no. 9, pp. 1884–1886, Sep. 2005.

[22] X. Chen, C. Li, and H. K. Tsang, "Fabrication-tolerant waveguide chirped grating coupler for coupling to a perfectly vertical optical fiber," *IEEE Photon. Technol. Lett.*, vol. 20, no. 23, pp. 1914–1916, Dec. 2008.

[23] J. Covey and R. T. Chen, "Efficient perfectly vertical fiber-to-chip grating coupler for silicon horizontal multiple slot waveguides," *Opt. Express*, vol. 21, pp. 10886–10896, 2013.

[24] G. Dabos, J. Bolten, A. Prinzen, A. L. Giesecke, N. Pleros, and D. Tsiokos, "Perfectly vertical and fully etched SOI grating couplers for TM polarization," *Opt. Commun.*, vol. 350, pp. 124–127, 2015.

[25] Y. Wang *et al.*, "Focusing sub-wavelength grating couplers with low back reflections for rapid prototyping of silicon photonic circuits," *Opt. Express*, vol. 22, pp. 20652–20662, 2014.

[26] D. Benedikovic *et al.*, "High-directionality fiber-chip grating coupler with interleaved trenches and subwavelength index-matching structure," *Opt. Lett.*, vol. 40, pp. 4190–4193, 2015.

[27] D. Taillaert, P. Bienstman, and R. Baets, "Compact efficient broadband grating coupler for silicon-on-insulator waveguides," *Opt. Lett.*, vol. 29, pp. 2749–2751, 2004.

[28] M. Antelius, K. B. Gylfason, and H. Sohlström, "An apodized SOI waveguide-to-fiber surface grating coupler for single lithography silicon photonics," *Opt. Express*, vol. 19, pp. 3592–3598, 2011.

[29] J. Smajic, C. Hafner, and D. Erni, "Optimization of photonic crystal structures," *J. Opt. Soc. Amer. A*, vol. 21, pp. 2223–2232, 2004.

[30] A. Dorodnyy, V. Shklover, L. Braginsky, C. Hafner, and J. Leuthold, "High-efficiency spectrum splitting for solar photovoltaics," *Solar Energy Mater. Solar Cells*, vol. 136, pp. 120–126, 2015.

[31] L. Alloatti and R. J. Ram, "Infrared vertically-illuminated photodiode for chip alignment feedback," *AIP Adv.*, vol. 6, 2016, Art. no. 085219.

Tatsuhiko Watanabe (M'12) was born in Japan, in 1989. He received the B.E., M.E., and Ph.D. degrees in engineering from Yokohama National University, Yokohama, Japan, in 2012, 2013, and 2016, respectively. From 2014 to 2017, he was a Research Fellow of the Japan society for the promotion of science, Tokyo, Japan. From 2016 to 2017, he was also a Fellow under the Japanese–Swiss Science and Technology Programme. He was with Institute of electromagnetic fields, ETH Zurich, Switzerland, as a Guest Researcher from 2016 to 2017, and is currently with them as a Fellow under the ETH postdoctoral fellowship from 2017.

His research interests include optical fibers and optical components for space division multiplexing and mode division multiplexing.

Masafumi Ayata was born in Japan, in 1990. He received the B.Sc. and M.Sc. degrees in electrical engineering and information systems from the University of Tokyo, Tokyo, Japan, in 2013 and 2015, respectively. He is currently working toward the Ph.D. degree at the Institute of Electromagnetic Fields, ETH Zurich, Zurich, Switzerland. His research interests include photonic integrated circuits, integrated plasmonic devices, and optical communications.

Ueli Koch received the M.Sc. degree in computational science and engineering from ETH Zurich, Zurich, Switzerland, in 2013. He is currently working toward the Ph.D. degree at the Institute of Electromagnetic Fields, ETH Zurich. His current research interests include the numerical modeling and simulation of surface effects in plasmonic nanostructures with a particular focus on electro-optic modulation.

Yuriy Fedoryshyn received the Master's degree in laser and optoelectronic technology from Lviv Polytechnic National University, Lviv, Ukraine, and the Ph.D. degree in electrical engineering from ETH Zurich, Zurich, Switzerland. He is currently leading the micro- and nanofabrication activities at the Institute of Electromagnetic Fields, ETH Zurich. His research interests include plasmonic and nanophotonic devices, including modulators, switches, detectors, and light sources.

Juerg Leuthold (F'13) was born in Switzerland, in 1966. He received the Ph.D. degree in physics from ETH Zürich, Zürich, Switzerland, for work in the field of integrated optics and all-optical communications. From 1999 to 2004, he was with Bell Labs, Lucent Technologies in Holmdel, USA, where he performed device and system research with III/V semiconductor and silicon optical bench materials for applications in high-speed telecommunications. From 2004 to 2013, he was a Full Professor at the Karlsruhe Institute of Technology, where he headed the Institute of Photonics and Quantum Electronics and the Helmholtz Institute of Microtechnology. Since March 2013, he has been a Full Professor at the Swiss Federal Institute of Technology (ETH), Zurich.